

Article

Monitoring of Gas Emissions in Light of an OEF Application

Victorin-Emilian Toader¹, Víctor Nicolae^{2,3,*}, Iren-Adelina Moldovan¹, Constantin Ionescu¹
and Alexandru Marmureanu¹

¹ National Institute for Earth Physics, Calugareni 12, RO077125 Magurele, Romania; victorin@infp.ro (V.-E.T.); iren@infp.ro (I.-A.M.); viorel@infp.ro (C.I.); marmura@infp.ro (A.M.)

² National Institute of Research and Development for Optoelectronics INOE2000, Atomistilor 409, RO77125 Magurele, Romania

³ Faculty of Physics, University of Bucharest, Atomistilor 405, RO77125 Magurele, Romania

* Correspondence: victor.nicolae@inoe.ro

Abstract: This study analyzes the possibility to use geophysical and geochemical parameters in an OEF (Operational Earthquake Forecasting) application correlated with short-term changes in seismicity rates using a magnitude–frequency relationship. Tectonic stress over the limits of rock elasticity generates earthquakes, but it is possible that the emission of gases increases as a result of the breaking process. The question is how reliable is the emission of radon-222 and Carbon Dioxide (CO₂), with effects on air ionization and aerosol concentration, in an OEF application? The first step is to select the seismic area (in our study this is the Vrancea area characterized by deep earthquakes at the bend of the Carpathian Mountains), then determine the daily and seasonal evolution of the forecast parameters, their deviations from the normal level, the short-term changes in seismicity rates using a magnitude–frequency relationship and finally to correlate the data with recorded seismic events. The results of anomaly detection, effect evaluation and data analysis alert the beneficiaries specialized in emergency situations (Inspectorate for Emergency Situations, organizations involved in managing special events). Standard methods such as the standard deviation from the mean value, time gradient, cross correlation, and linear regression are customized for the geological specificity of the area under investigation. For detection we use the short-time-average through long-time-average trigger (STA/LTA) method on time-integral data and the daily–seasonal variation of parameters is correlated with atmospheric conditions to avoid false decisions. The probability and epistemic uncertainty of the gas emissions resulting from this study, in addition to other precursor factors such as air ionization, time between earthquakes, temperature in the borehole, telluric currents, and Gutenberg Richter “a-b” parameters, act as inputs into a logical decision tree, indicating the possibility of implementing an OEF application for the Vrancea area. This study is novel in its analysis of the Vrancea area and performs a seismic forecasting procedure in a new form compared to the known ones.

Keywords: radon anomalies; multidisciplinary monitoring; precursor phenomena; air ionization monitoring; CO₂ monitoring; OEF; anomaly detection



Citation: Toader, V.-E.; Nicolae, V.; Moldovan, I.-A.; Ionescu, C.; Marmureanu, A. Monitoring of Gas Emissions in Light of an OEF Application. *Atmosphere* **2021**, *12*, 26. <https://doi.org/10.3390/atmos12010026>

Received: 7 August 2020

Accepted: 12 October 2020

Published: 27 December 2020

Publisher’s Note: MDPI stays neutral with regard to jurisdictional claims in published maps and institutional affiliations.



Copyright: © 2020 by the authors. Licensee MDPI, Basel, Switzerland. This article is an open access article distributed under the terms and conditions of the Creative Commons Attribution (CC BY) license (<https://creativecommons.org/licenses/by/4.0/>).

1. Introduction

An OEF (Operational Earthquake Forecasting) application is based on the real-time monitoring of geophysical and geochemical parameters as well as the long-term data analysis. In this context, the monitoring of gas emissions due to tectonic stress could be an important component in making decisions to reduce losses caused by a seismic event. S. Pulinets Sergey and D. Ouzounov point out in [1] the meaning of short-term earthquake forecasts and the role of gas interaction between the lithosphere and the atmosphere. These gas emanations result in air ionization and ultimately to seismically induced aerosols. This study is a more deterministic approach to the forecast with respect to the presently available purely probabilistic OEF models because it is more heavily based on the analysis

of precursors in real time and offline. The Italian radon monitoring network of soil radon emission [2,3] or the continuous monitoring of soil CO₂ in Japan [4] are examples of such an approach. This does not exclude statistical analysis such as the detection of hydrogeochemical seismic precursors [5] or uncertainty evaluation in seismic risk assessments [6]. The monitoring of earthquake precursors by multidisciplinary stations is the usual solution [7] as well as a data analysis according to the geological specificity of the monitored area [8]. The gas emission is correlated with seismic events [9,10], volcanic [11,12] and geothermal activity [13–15] and is considered a precursor factor [16,17]. The best results are obtained in areas with faults [18,19] or mud volcanoes [20–23].

Our study looks into the monitoring of gas emissions with the goal to develop an OEF application for the Vrancea area, which is characterized by deep earthquakes at the bend of the Carpathian Mountains. The main difference from the analysis conducted in the mentioned articles and the increased difficulty it brings is that the gas source cannot be present at depths greater than 60 km where the earthquakes are located. The half-life of radon is 3.82 days and its mobility in the ground by diffusion is limited, too. Near the monitored area there are mud volcanoes that emit gases [20,24]. A possible explanation is that the concentrated tectonic stress at depths over 60 km is progressively transmitted to the surface and favors the emission of gases in the fault areas. This process depends on the barometric pressure, humidity, soil temperature, and solar radiation, all of which vary with the seasons. A higher temperature has the effect of expanding the microfractures which can cause a release of gases (radon, CO₂). An increase in pressure on the rocks results in an increase in temperature. N. Frunzeti et al. [20] make an analysis of radon emissions to soil and water globally and note that the upward flow of gases may be a result of the Bernoulli effect. These hypotheses are difficult to verify but the source of the gases is not located in the hypocenter of the earthquake and the measured effects depend on atmospheric conditions. The data we have analyzed also show the presence of CO, which can be explained by the atmospheric short-range transport from nearby polluted urban areas. For this reason, it is important that the choice of monitoring location be made after a geological study in the fault areas. A radon level assessment in relation to seismic events in the Vrancea region is the title and subject of the article [25], which studies the same area as in our study but with different equipment and in a previous timeframe. In this article the “radon concentration was examined between the mean values and plus/minus two standard deviations”. In our study we compare this method with other detection algorithms such as short-time-average through long-time-average trigger (STA/LTA) applied on signal integration.

This study indicates the possibility of including the monitoring of gas emissions (radon-222, CO₂) in a complex OEF system, with applications for the Vrancea seismic zone and the transmission of information in the existing seismic warning network. Such a decision-making system could be useful in risk mitigation actions [26]. The statement “Clearly, any practical use of forecasting methods must be done in an appropriate policy framework, one that can weigh costs against benefits and potential gains against possible risks” [27] also applies in our case.

2. Monitoring Network

The multidisciplinary monitoring network of the NIEP (National Institute for Earth Physics) includes five stations measuring radon, CO₂, CO, air ionization, atmospheric electrostatic field, earth and magnetic field, temperature in the borehole, meteorological station, solar radiation, telluric field in addition to seismic speed and acceleration sensors. The monitored area is characterized by faults (an example in Discussion and Conclusions paragraph) and in the southern part by muddy volcanoes. Figure 1 presents the seismicity of the area where deep earthquakes occur (marked in dark blue) and the name and position of the stations used in this study.

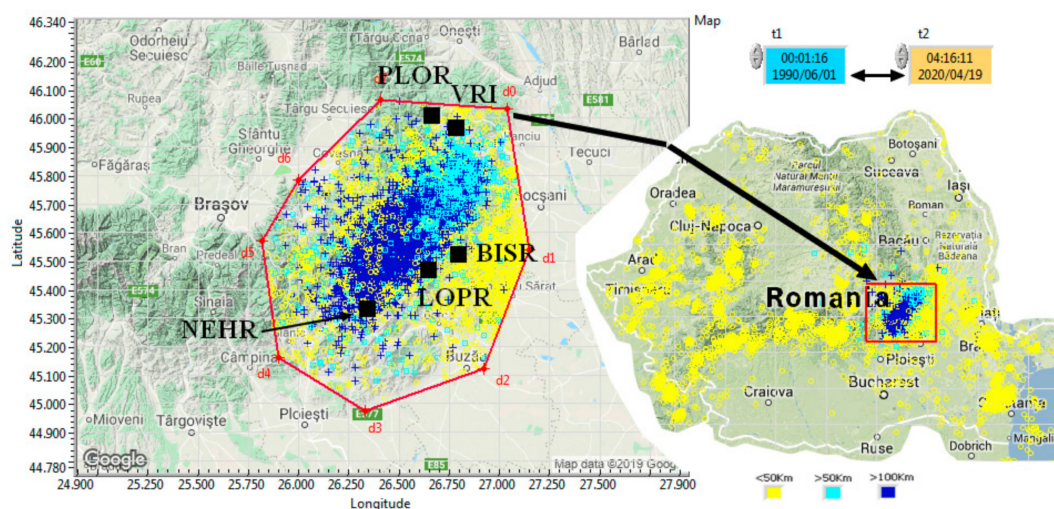


Figure 1. Romania and Vrancea seismicity 2014–2020, gas monitoring network.

Table 1 details the monitoring structure. Each location has a unique identification code that allows access to data on the <http://geobs.infp.ro/platform>.

Table 1. Monitoring stations and their equipment.

Station Name Lat/Lon	Code	Equipment	Sampling Period
Bisoca BISR 45.54811/26.7099	BISRd	Radon equipment with inclinometer, air temperature, pressure and humidity	3 h
	BISRCO2	CO ₂ , CO, air temperature, humidity, and meteorological station	1 s
Lopatari LOPR 45.4738/26.568	LOPRd	Radon equipment with inclinometer, air temperature, pressure and humidity	3 h
	LOPrCO2	CO ₂ , CO, air temperature, humidity	1 s
Nehoiu NEHR 45.4272/26.2952	NEHRd	Radon equipment with inclinometer, air temperature, pressure and humidity	3 h
	NhCO ₂	CO ₂ , CO, air temperature, humidity, and meteorological station	1 s
	Ions+	Air +ions counter	1 s
	Ions-	Air -ions counter	1 s
Plostina PLOR 45.8512/26.6498	PLRd2	Radon equipment with inclinometer, air temperature, and humidity	3 h
	Tf	Borehole temperature, HART 5 protocol	1 s
	Tforaj	Borehole temperature	1 s
	PLT0, PLT1	Telluric currents	0.1 s
Vrancioaia VRI 45.8657/26.7277	VRI d	Radon equipment with inclinometer, air temperature, pressure and humidity	3 h
	VRIco2	CO ₂ , CO, air temperature, humidity, and meteorological station	1 s

The radon detector Radon-Scout PLUS is produced by SARAD. The measuring range is up to 10 MBq/m³, sensitivity 1.8 cpm @ 1000 Bq/m³ independent of humidity, and the working temperature is −20 to 40 °C. The measurement chamber, equipped with a semiconductor detector and high voltage collection, is immune to ambient humidity. The unit includes a barometer (800–1200 mbar), a temperature sensor, a humidity sensor and an

inclinometer. The sample rate is 3 h. CO₂ and CO monitoring was conducted in real time. This information along with humidity, temperature and dew point were measured with DL 302–DL303 produced by ICPDAS. Its specifications are: range 0 to 9999 for CO₂, resolution 1 ppm, accuracy ± 30 ppm, response time 20 s, range -10 to 50 °C, and resolution 0.1 °C. The sample rate is 1 s. The borehole was performed for seismic measurements, was filled with water and includes an accelerometer and a temperature sensor.

3. Data, Methods, Procedure

3.1. Data and Detection Methods

Data monitoring was conducted through independent acquisition systems that perform the first level of detection based on the trigger and dettrigger levels with real-time message transmission to the <http://geobs.infp.ro/web> platform. The radon-222 monitoring equipment is autonomous, having the ability to stay connected on batteries for 2 months. The data were then downloaded manually using a software application from the device manufacturer. The information was processed automatically and transformed into a format compatible with the other data, namely ASCII text with a TAB delimiter. The analysis program converted the sampling periods from Table 1 to 1 min for large amounts of information. The data were saved in 1 h files which were transmitted to a database and viewed/queried through the <http://geobs.infp.ro/platform>.

An example of STA/LTA events detection [28–31] is shown in the Figure 2.

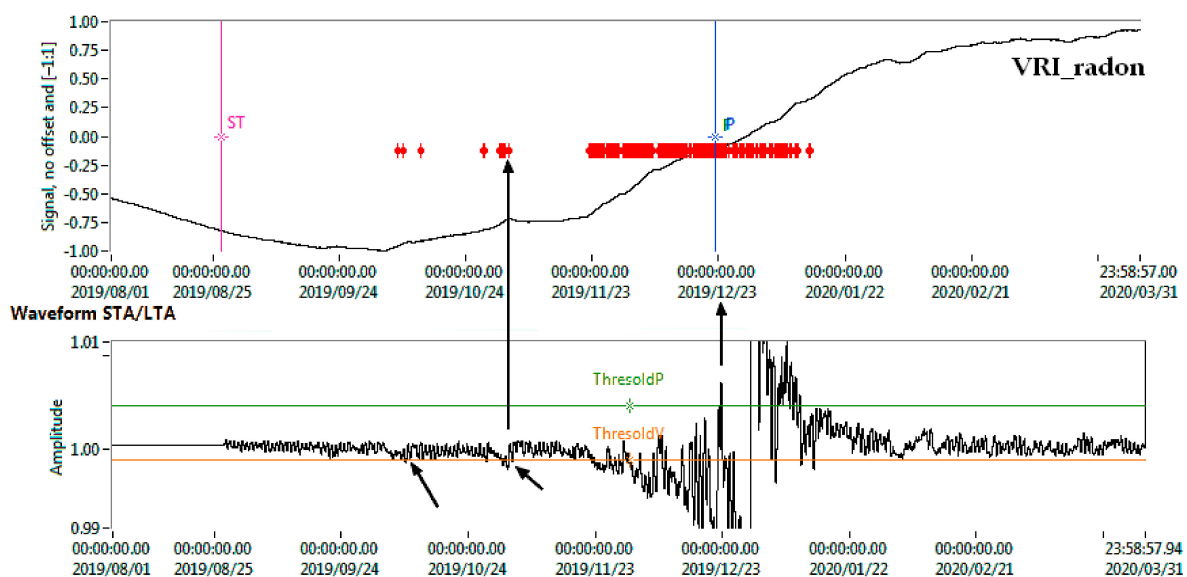


Figure 2. Anomaly detection using short-time-average through long-time-average (STA/LTA) triggering algorithm.

Three methods were used: PC-SUDS, Processing of Seismic Data Stored in the Seismic Unified Data System, [32,33], Allen [34], and Hilbert transforms, which correlated with the envelope function [35]. The PC-SUDS was used for the seismic detection of the P wave. This method is useful for faster signals (100 Hz sample rate). For very low signals the Hilbert method is better (days sample rate). For our case the equivalent sample rate used was 60 s and we acquired good results with the STA/LTA method. This value was also used to integrate signals. Even if the data acquisition was conducted at 1 s, we used sampling periods of 60 s for the analysis of longer periods of time. Figure 2 shows the result of the Allen STA/LTA method with two limits—threshold pick and threshold valley, which were applied to the integral radon signal. In this case, we used two time windows and calculated the sum of the samples power for the two cases. Finally, we made the ratio between them (STA/LTA) and the result is a time function that indicates the signal anomalies. Depending on the case (radon, CO₂, temperature), the two time windows were dimensioned.

The authors of [36] describe the methods for detecting anomalies applied to radon time series in correlation with seismicity. The standard deviation from the mean value, and the relationship between radon and seismicity are presented in Figure 3.

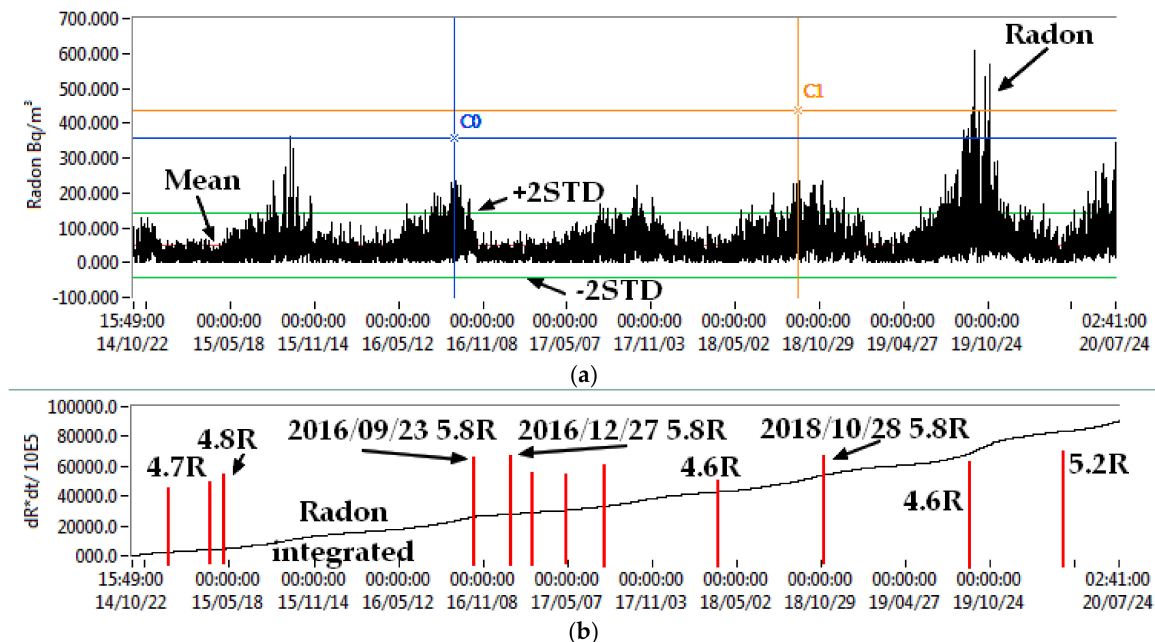


Figure 3. Radon evolution in Bisoca station: (a) radon time series, ± 2 STD standard deviations method, mean value; (b) integral of radon and correlation with seismicity.

In Figure 3a the standard deviation and mean values are shown for the whole period of time. Normally, this is carried out over limited periods of time in cycles in which the analyzed parameter varies. Figure 3a shows that the maximum annual variations are in November for Bisoca station. The intersections between the radon signal and the ± 2 STD are not always correlated with seismicity (Figure 3). Seasonal variations introduce errors in the application of this method. These could be eliminated by applying this detection of anomalies for shorter periods of time or by filtering seasonal variations. In the procedure described in the next paragraph, the analysis is conducted daily and seasonally to reduce false detections. Figure 3b shows the correlation between seismicity and the integral of the radon signal. We chose this method to highlight the dependence of radon concentration on time.

3.2. OEF Procedure

The OEF procedure is general and involves the following steps: (1) select the seismic area (Figure 1); (2) determine the a , b parameter from Gutenberg Richter law [37–41], and other forecast parameters such as air ionization, radon concentration, CO_2 , temperature in borehole, telluric field; (3) compare the seismicity with precursor factors (geophysics, geochemical) and determine the probability and epistemic uncertain forecast time; (4) evaluate the emergency state using a logic tree; (5) decide the event state and send the information.

For this purpose, we developed two software applications that allow the updating of the predicted seismicity according to the real one and analyze the precursor factors. Part of the seismic information comes from ISC web site: International Seismological Centre, Online Bulletin, <http://www.isc.ac.uk>, Internatl. Seismol. Cent., Thatcham, United Kingdom, 2016, Romplus Catalog, and from EMSC (European-Mediterranean Seismological Centre).

(1.) Select the seismic area:

For the selection of the seismic zone, a large area was initially selected, after which we chose the area of interest. In this stage it is necessary to have geological information. The location of the sensors was established in the faulty areas (see Discussion and Conclusions

paragraph) where it is estimated that the gas emission will be higher (radon concentration is one of precursor factor). A seismic analysis requires data from a catalog or from the ISC (International Seismological Centre). In Figure 1, the selected area is marked with a red polygon and the method can be applied to any area for which the ISC provides the required data. The preparation zone is also used to establish the area of interest. This is determined using an empiric of Dobrovolsky [42] formula.

(2.) Determine short-term changes in seismicity rates using the Gutenberg Richter magnitude–frequency relationship and the daily–seasonal evolution of forecast parameters:

The Gutenberg Richter (GR) law [37–41] states that earthquake magnitudes are distributed exponentially as

$$\text{Log}_{10} N(m) = a - b \cdot m \tag{1}$$

where $N(m)$ is the number of earthquakes with a magnitude larger or equal to “ m ”, “ b ” is a scaling parameter and “ a ” is a constant. We use the least square regression method for determining “ a ” and “ b ”. The magnitude of completeness M_c is determined by applying a regression algorithm until the error starts to grow.

Detection algorithms use both level and duration thresholds (Figure 2, STA/LTA case) to highlight deviations from the norm. The choice of these parameters is also made according to the daily (night–day) and seasonal variations [43]. Even if the analysis is carried out over the same season, differences may occur. We chose the years 2017, marked with (a), and 2018, marked with (b), in order to highlight the annual variations of radon and CO₂ in Bisoca and Nehoiu, respectively. Figures 4–7 present radon variation in Bisoca station in spring, summer, autumn and winter and Figures 8–11 represent the CO₂ variations in Nehoiu. Radon registers higher values at midnight in the warm period of the year and becomes uniform before decreasing in winter. CO₂ has a similar behavior. Figure 6b shows an increase in radon preceding the earthquake with a magnitude of 5.8R. In the case of CO₂, Figures 9a and 10b indicate a maximum of CO₂ before the seismic event at a time of day when it should have decreased. This type of analysis requires a large amount of information in order to eliminate false decisions.

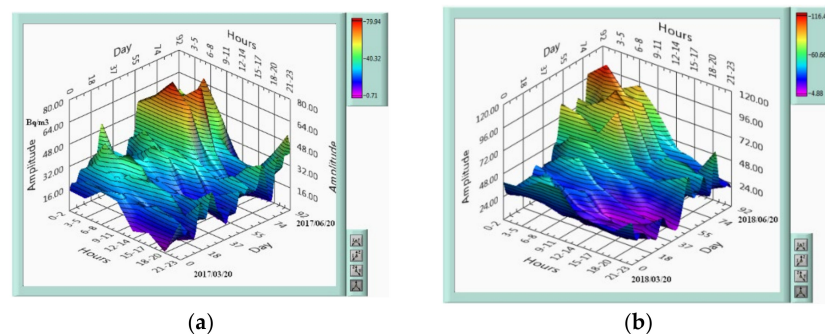


Figure 4. Radon evolution in Bisoca station spring: (a) 2017; (b) 2018.

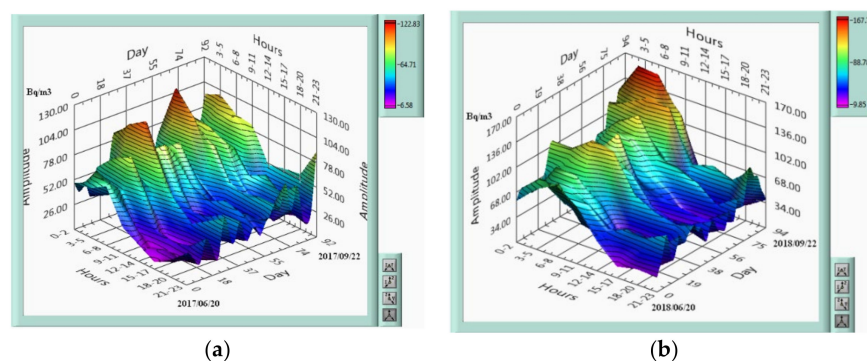


Figure 5. Radon evolution in Bisoca station, summer: (a) 2017; (b) 2018.

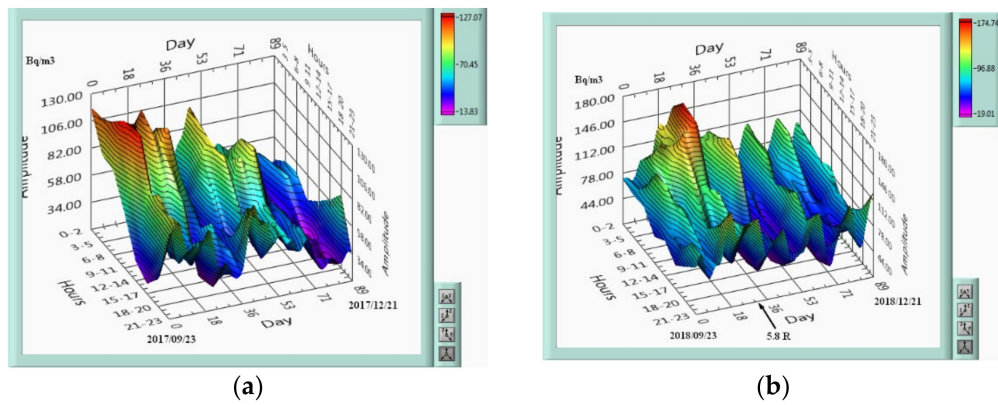


Figure 6. Radon evolution in Bisoca station, autumn: (a) 2017; (b) 2018.

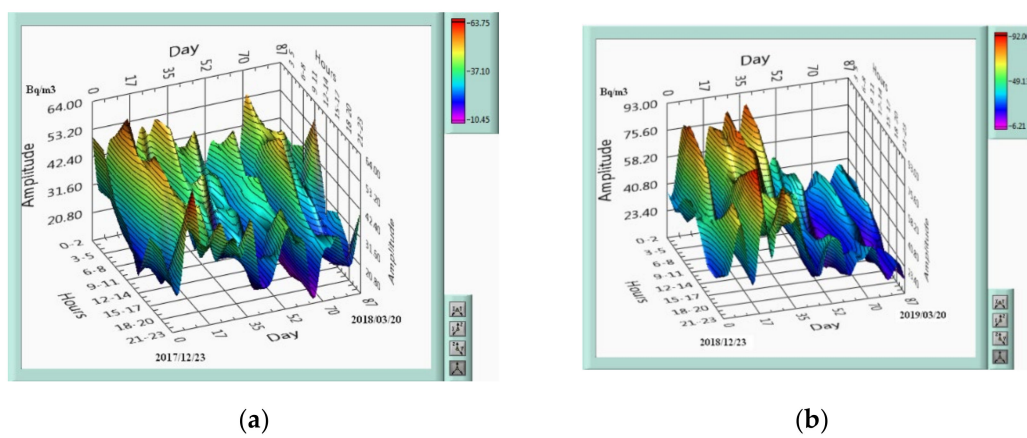


Figure 7. Radon evolution in Bisoca station, winter: (a) 2017; (b) 2018.

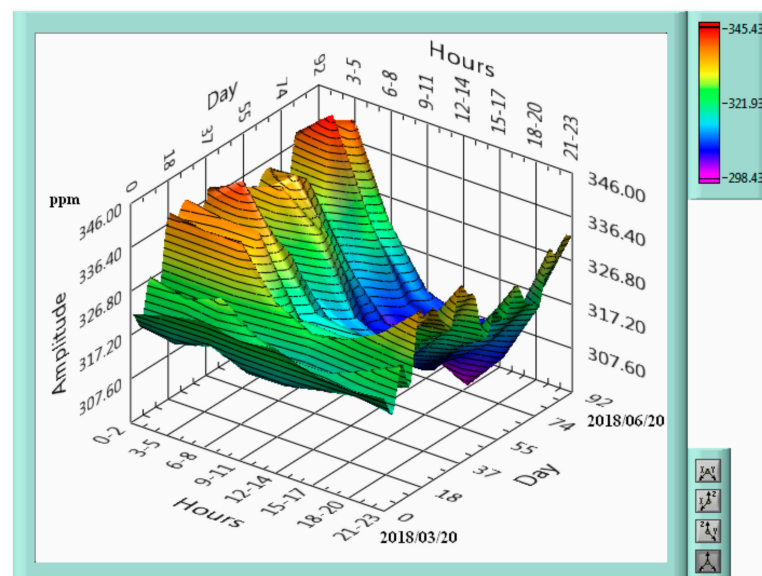


Figure 8. CO₂ in Nehoiu spring 2018.

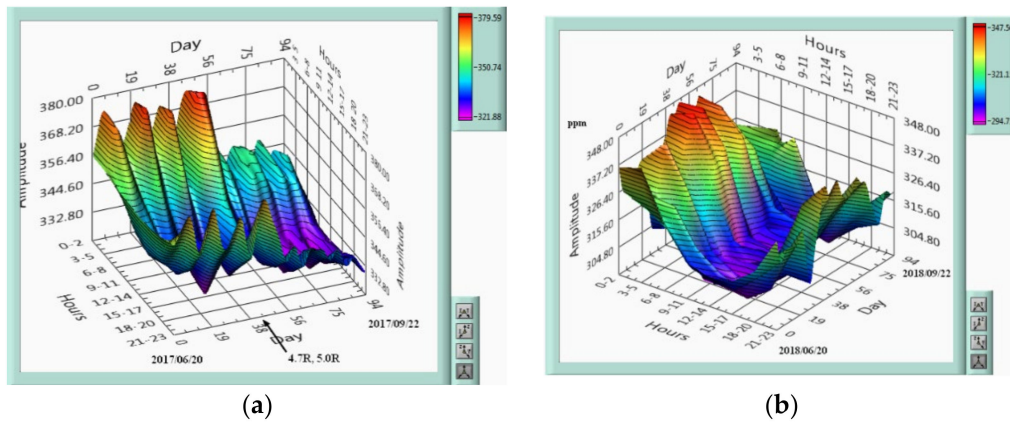


Figure 9. CO₂ in Nehoiu summer: (a) 2017; (b) 2018.

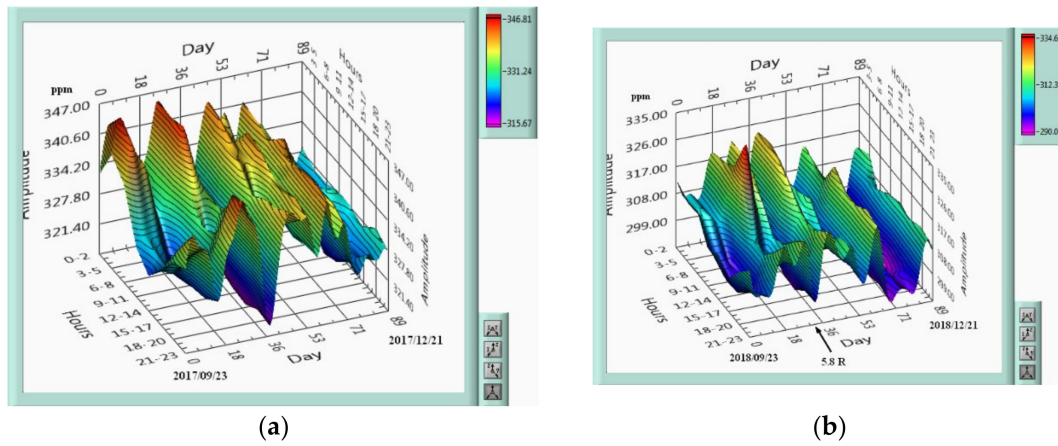


Figure 10. CO₂ in Nehoiu autumn: (a) 2017; (b) 2018.

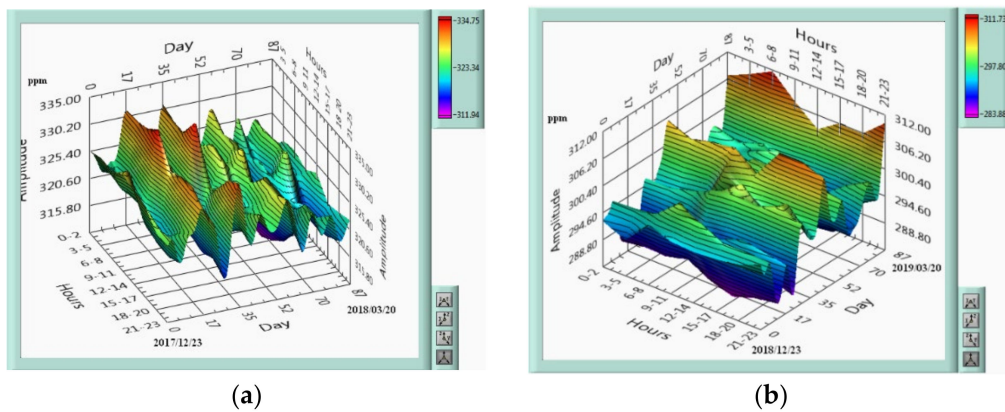


Figure 11. CO₂ in Nehoiu winter: (a) 2017; (b) 2018.

A high variation of radon or CO₂ could be seasonal without having a connection with seismicity. If a variation of the GR parameters is superimposed in this case, it can lead to a false decision. A machine learning method could be a solution to this problem [36].

(3.) Compare the seismicity with precursors factors (geophysics, geochemical) and determine the probability and the epistemic uncertain forecast time:

Figure 12 presents in the same plot the geophysical information next to GR “a-b” evolution for Vrancea area in period 2018–2020/03/31. The signals related to gas emission and air ionization are time integral (“*dt” notation on graphs is 60 s) to incorporate the effect of accumulations over time. The first trace, BISRd (see Table 1), represents the

time series of radon but the detection was performed on the integral signal because this method is more efficient. The following signals represent the radon in Lopatari, Nehoiu, Vranceaia and Plostina. The magnitude is M_{dpvs_M} and is higher when the GR a-b is low long time. Air ionization ($NhCOb_Iop$, $NhCOb_Ion$) and CO_2 ($NhCOb_Co2$) are measured from Nehoiu station. The temperature in a borehole (Table 1, Tf and $Tforaj$ in PLOR station) is a precursor factor analyzed in Figure 12 along with the gas emission. In all stations we also have meteorological information. The measured values should be corrected with temperature, humidity and atmospheric pressure. The equipment that determines the concentration of radon and CO_2 have these sensors embedded in order to make these corrections. For a general analysis we consider that the monitored area is small and homogeneous from a meteorological point of view. Sometimes this is not always the case. Monitoring stations are located in isolated areas near villages where no polluting industrial activities take place that could affect our measurements. However, in two cases we were surprised to find the presence of CO , indicating pollution. These situations were partially explained (in one case a saw was propelled by a diesel engine near the monitoring station, and in another there were live fires due to natural well gas emissions in the Lopatari area). In the first situation it was decided to move the sensors (Vranceaia) and for the second case (Lopatari) the research was at the beginning. For a more detailed analysis we have information about the movement of clouds and their electrostatic charge through a network of radars (Boltek equipment).

The correlation between GR and seismicity is presented in Figure 13. The time between the moments of earthquakes (ΔT , Figure 13) is useful but it indicates an increase in seismicity not necessarily an event. So, when the GR-a decreases to an approximate value of 2.9 (a minimum for Vrancea) for a period longer than 41 days we will have a seismic with $M_w > 4.5$. GR a-b were calculated on a 10-week window and with a 1-week (7-day) step.

We calculate the probability and epistemic uncertain forecast time shown, for example, in Figure 12. The results can be found in Table 2, while the determination data are presented in Table 3. It is important to take into consideration the distance between the measuring location and the hypocenter of the earthquake. S. Süer et al. in [44] demonstrate that the concentration of radon-222 at an active fault is correlated with the total earthquake energy (TEE). This parameter is inversely proportional to the square of the hypocenter distance. For this reason there are differences between the values determined in Table 2. These differences can be minimized with a proper selection of the investigated area. The choice of the monitoring area was made according to the preparation zone determined by the Dobrovolsky [42] formula. The GR a-b parameters were included in the table because they represent the magnitude–frequency relationship used by OEF applications (Figure 13).

Table 2. Probability of true/false detections, uncertain and average of times between the detection of radon, Gutenberg Richter a-b, ions, CO_2 , temperature in borehole.

Time 1 January 2018 31 March 2020	Stations Radon-222					GR a-b	Ions+	Ions-	CO ₂	Tf
	BISRd	LOPRd	NEHRd	VRId	PLRd2					
Location	BISRd	LOPRd	NEHRd	VRId	PLRd2	-	NEHR	NEHR	NEHR	PLOR
Probability	0.57 4 TRUE/ 7 TOTAL	0.29 4/14	0.40 4/10	0.50 4/8	0.44 4/9	0.50 3/6	0.57 4/7	0.50 4/8	0.57 4/7	0.57 4/7
Uncertain (STD)	4.98	3.93	1.15	14.87	2.70	5.92	9.74	8.88	3.09	37.71
Weight	0.18	0.14	0.04	0.54	0.1	1	0.5	0.5	1	1
Average Time (Days)	16.5	10.03	9.9	30.65	10.63	13.3	26.25	27.75	18.43	45.45

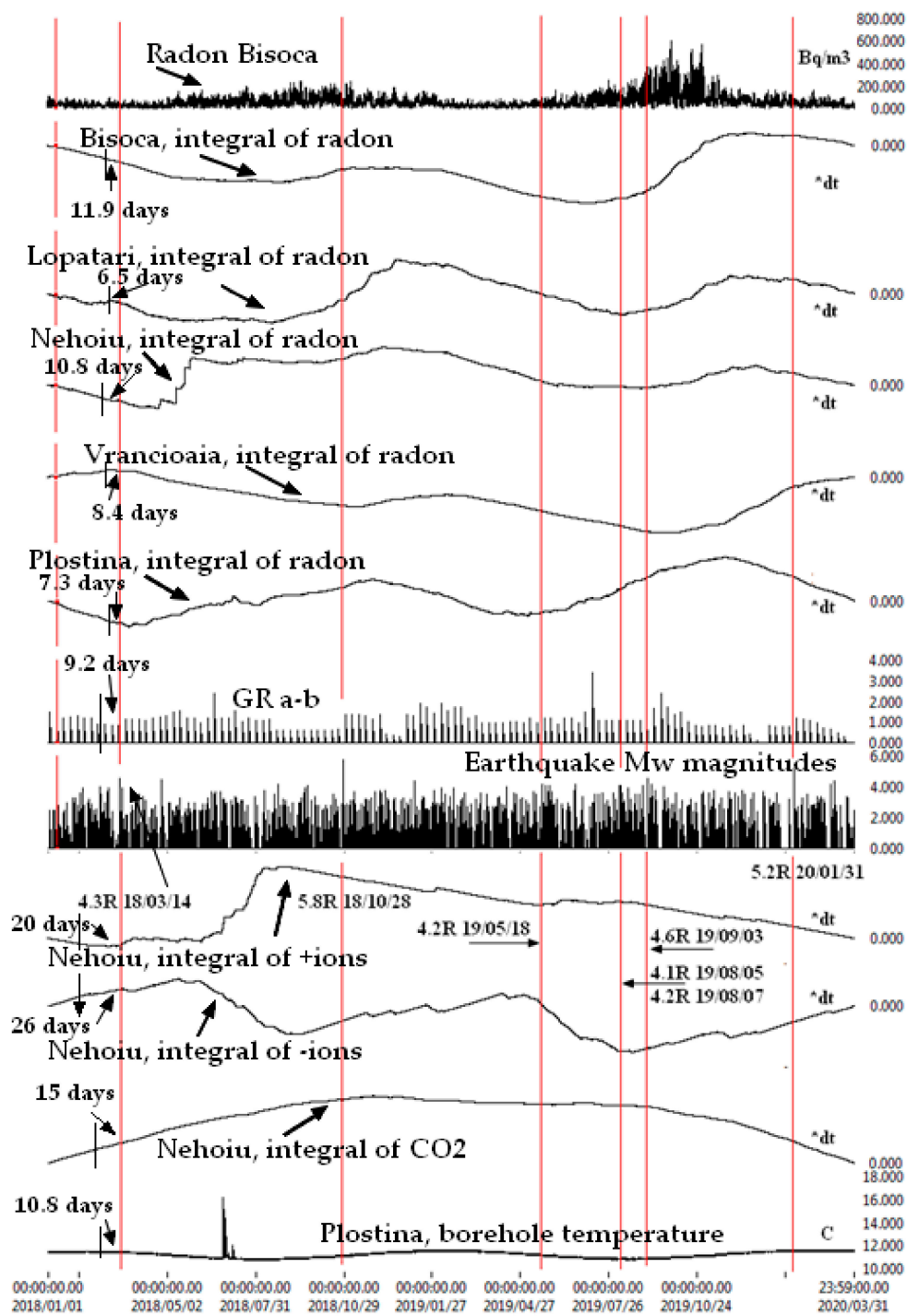


Figure 12. Vrancea area, radon, Gutenberg Richter (GR) a-b, Mw, Ions+/-, CO₂, temperature in borehole.

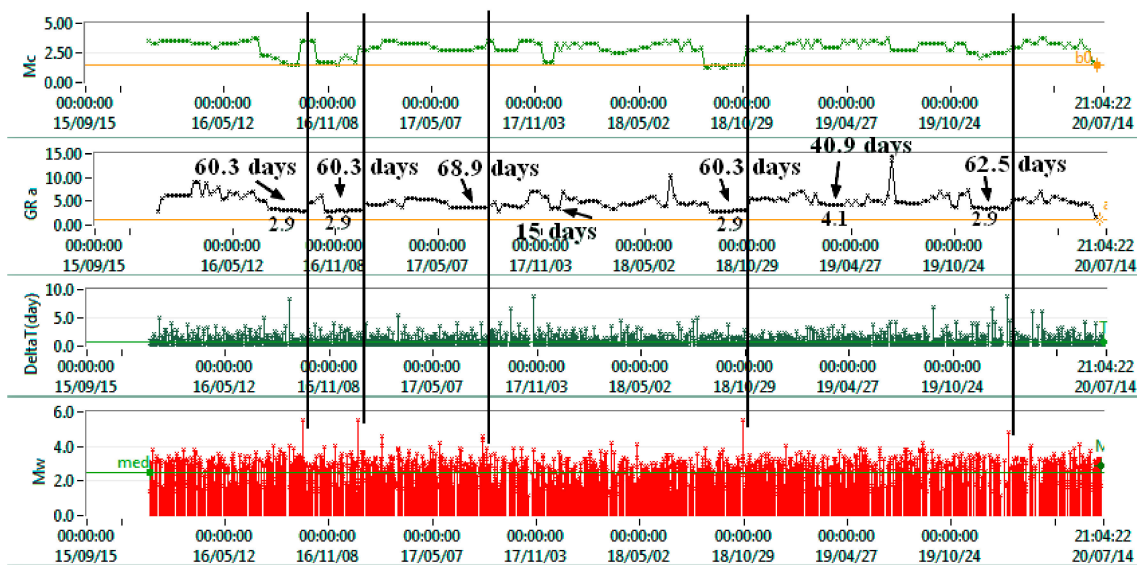


Figure 13. The relationship between Vrancea seismicity and Gutenberg Richter parameters a-b, and the magnitude of completeness M_c .

Table 2 is the result of the analysis of evolution of all parameters from Figure 12. We measured the time determined by the detection of precursor anomalies and the moments at which the earthquakes occurred. We decide with TRUE (1) the cases in which, after an anomaly, we had an earthquake and false otherwise, FALSE (0). The total number of 1 over the all determinations is the probability from Table 2. The standard deviation of forecast times (TRUE cases) is the epistemic uncertainty [45]. For example, for radon we have 20 of TRUE values from 48 determinations (Table 3) and 4 out of 7 cases for BISRD. The uncertainty of the time forecast related to radon in Bisoca (BISRd) is determined by 11.9, 20.4, 21.2, 12.5 forecast days corresponding to the 4 earthquakes produced in the analyzed time interval (Table 3). We select earthquakes greater than 4.6R in the area marked in red in Figure 1.

In Table 3, slope + means a rising curve, max a maximum value and “dt” a deviation visible using a derivative function.

The detection of events is realized in two steps: in real time directly in the monitoring area and second offline with specialized software that generates graphs such as the ones in Figures 12 and 13. The first detection aims to draw attention to an event. This is analogous to the difference between the first localization of an earthquake (which is normally carried out automatically) and its revision (what you can find at International Seismological Centre ISC or in a seismic catalog). The web platform <http://geobs.infp.ro/> displays real-time warnings and parameter values over 5 min, such as those in Figure 14.

CO2

Station	CO(ppm)	CO2(ppm)	Humidity(%)	Temp(C)	Tdewpoint(C)	Time
VRI	0.000	455.000	39.340	17.390	3.400	20/04/28 14:15:59

Statie: VRIco2 - 20/04/28 07:38:21 Tc 15.000>=15.000

Figure 14. Information on <http://geobs.infp.ro/> web platform in real time.

Table 3. Detection of events, time forecast, correlation with seismicity (TRUE = 1 trigger followed by earthquake, FALSE = 0 trigger without earthquake).

Event Detection yy/mm/dd	Magnitude (R)/Depth	Epicentral Distance from the Station (km)	Parameter	Trigger	Time Forecast (Days)	N TRUE = 1/FALSE = 0
18/01/26			Radon NEHRd			0
18/01/15			Radon LOPRd			0
18/02/18			Radon PLRd2			0
18/05/09			Radon VRId			0
18/03/14	4.6/ 137 Km	17.3	Radon BISRd	slope-,dt	11.9	1
		24.23	Radon LOPRd	slope-,dt	6.5	1
		35.3	Radon NEHRd	slope-,dt	10.8	1
		26.68	Radon VRId	slope-,dt	8.4	1
		31.5	Radon PLRd2	slope-,dt	7.3	1
			GR a-b	slope+,dt	9.2	1
		35.3	+Ions NEHR	slope-, min	20	1
		35.3	-Ions NEHR	slope+, max	26	1
		35.3	NhCO ₂	slope-,dt	15	1
	31.5	Tf PLOR	dt	10.8	1	
2018/06/14			GR a-b			0
2018/06/27			Tf PLOR			0
2018/07/02			Radon VRId			0
2018/07/08			Radon NEHRd			0
2018/07/08			Radon NEHRd			0
2018/07/17			NhCO ₂			0
2018/08/16			Radon PLRd2			0

Table 3. Cont.

Event Detection yy/mm/dd	Magnitude (R)/Depth	Epicentral Distance from the Station (km)	Parameter	Trigger	Time Forecast (Days)	N TRUE = 1/FALSE = 0
2018/09/29			Radon LOPRd			0
2018/10/16			Radon LOPRd			0
18/10/28	5.8/ 148 Km	30.96	Radon BISRd	slope+,dt	20.4	1
		20.52	Radon LOPRd	slope+,dt	9.6	1
		21.12	Radon NEHRd	slope+,dt	9.6	1
		40.07	Radon VRId	slope-,dt	39.6	1
		37.56	Radon PLRd2	slope+,dt	13.2	1
			GR a-b	slope+,dt	12	1
		21.12	Ions+ Nehoiu	slope-	33	1
		21.12	Ions- Nehoiu	slope+	33	1
		21.12	NhCO ₂	slope-,dt	21	1
		40.77	Tf PLOR	dt	56	1
18/11/18			Radon LOPRd			0
18/11/28			+Ions NEHR			0
18/11/28			-Ions NEHR			0
18/12/07			Radon LOPRd			0
18/12/16			NhCO ₂			0
18/12/21			-Ions NEHR			0
19/01/08			Tf PLOR			0
19/01/12			Radon BISRd			0
19/01/30			+Ions NEHR			0
19/01/30			-Ions NEHR			0
19/02/15			Radon NEHRd			0

Table 3. Cont.

Event Detection yy/mm/dd	Magnitude (R)/Depth	Epicentral Distance from the Station (km)	Parameter	Trigger	Time Forecast (Days)	N TRUE = 1/FALSE = 0
19/02/18			Radon LOPRd			0
19/04/07			+Ions Nehoiu			0
19/04/07			-Ions Nehoiu			0
19/04/13			Radon LOPRd			0
19/04/22			Radon VRId			0
19/05/21			GR a-b			0
19/07/14			Radon PLRd2			0
		37.23	Radon BISRd	slope+,dt	21.2	1
		24.5	Radon LOPRd	slope+,dt	15.6	1
		7.16	Radon NEHRd	slope+,dt	8.4	1
		57.39	Radon VRId	slope-,dt	37.3	1
		54.41	Radon PLRd2	slope+,dt	9.6	1
19/09/03	4.6/ 119 Km		GR a-b	slope+,dt	10	1
		7.16	+Ions NEHR	slope-, max	16	1
		7.16	-Ions NEHR	slope+, min	16	1
		7.16	NhCO ₂	slope-,dt	19.3	1
		54.41	Tf PLOR	dt	94	1
19/09/09			Radon BISRd			0
19/10/09			Radon PLRd2			0
19/10/14			Radon NEHRd			0
19/10/08			Radon BISRd			0
19/10/31			Radon BISRd			0
19/10/18			Radon LOPRd			0
19/10/25			NhCO ₂			0

Table 3. Cont.

Event Detection yy/mm/dd	Magnitude (R)/Depth	Epicentral Distance from the Station (km)	Parameter	Trigger	Time Forecast (Days)	N TRUE = 1/FALSE = 0
19/10/27			Tf PLOR			0
19/11/05			Radon VRId			0
19/11/05			GR a-b			0
19/11/13			Radon LOPRd			0
19/12/15			Radon PLRd2			0
19/12/31			Radon LOPRd			0
		14.19	Radon BISRd	slope-,dt	12.5	1
		24.87	Radon LOPRd	slope-,dt	8.4	1
		40.53	Radon NEHRd	slope-,dt	10.8	1
		20.18	Radon VRId	slope+,dt	37.3	1
		21.87	Radon PLRd2	slope-,dt	12.4	1
20/01/31	5.4/ 118 Km		GR a-b	slope+,dt	22	1
		40.53	+Ions NEHR	slope-, max	36	1
		40.53	-Ions NEHR	slope+, min	36	1
		40.53	NhCO ₂	slope-,dt	55	1
		21.87	Tf PLOR	dt	21	1

Another method of analysis and detection is cross correlation [46]. An example is in Figure 15, in which we analyze the CO₂ correlation in Vrancioaia and Nehoiu before producing a 5.2R earthquake. The results may be better in case of higher seismicity. V.D. Rusov et al. in [47] use a cross correlation between radon and magnetic field. The common element is the temperature on which the radon concentration depends, but which also has a local piezoelectric effect that modifies the magnetic and telluric fields.

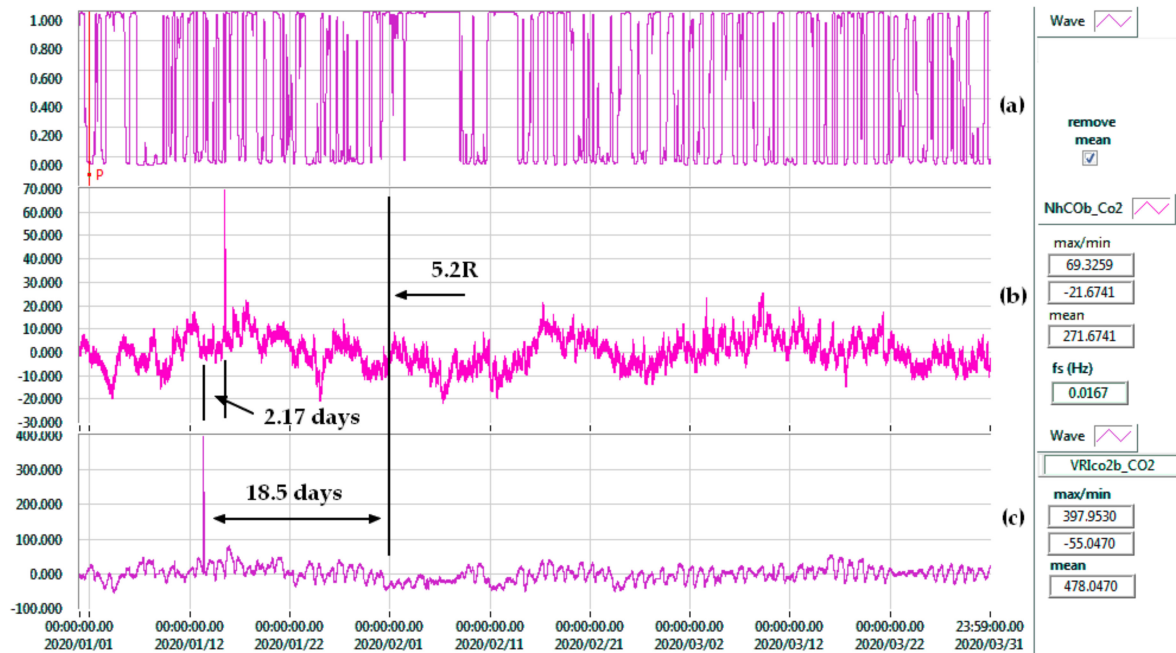


Figure 15. Comparative analysis of time series: (a) cross correlation (similar with Excel's function CORREL) of CO₂ from Nehoiu (b) and CO₂ from Vrancioaia (c).

The gas emission depends on the soil temperature which is correlated with the solar radiation [48]. In Plostina station we have a net radiometer (Table 1) to determine the direct and reflected solar radiation that allows the determination of the soil temperature. A study [49] showed a correlation between seismicity and albedo. As a result, solar radiation is also a factor to consider in a decision logic tree.

The radon, CO₂, +ions+ and -ions graphs from this study represent the filtered values of time series with 1 min-resolution. In Table 1 each parameter has a defined sampling rate ranging from 3 h to 0.1 s. Higher sampling frequencies are useful in spectral analysis but a 1 min sampling period is optimal in analyzing data over long periods of time without a significant loss of information affecting the detection of events.

(4.) Evaluate the emergency state using a logic tree:

The probabilities and epistemic uncertainties from Table 2 form the foundation of a decision in a logical tree. Epistemic uncertainties were quantified for gas emissions, temperature in the borehole in correlation with GR a-b parameters that represent the short-term changes in seismicity rates. The answer to how a logical tree would work for geophysical and geochemical parameters can only be given by experimentation. A decision-maker requires certain information in order to declare a seismic event and take actions to mitigate the effects in a cost-benefit approach. Seismic sources and the monitoring network involved in this study are presented in Figure 1. The result of Table 2 can be presented in the form of a logical tree with weights associated for each parameter. Bommer et al. [50] presents transparent weighting procedures for logical tree branches. Probabilities can be used in other vote-based methods, such as many seismic digitizers [33]. In the case of

Table 2, the weights were calculated using the criterion that the sum of the branches is 1 in the logical tree (Figure 16).

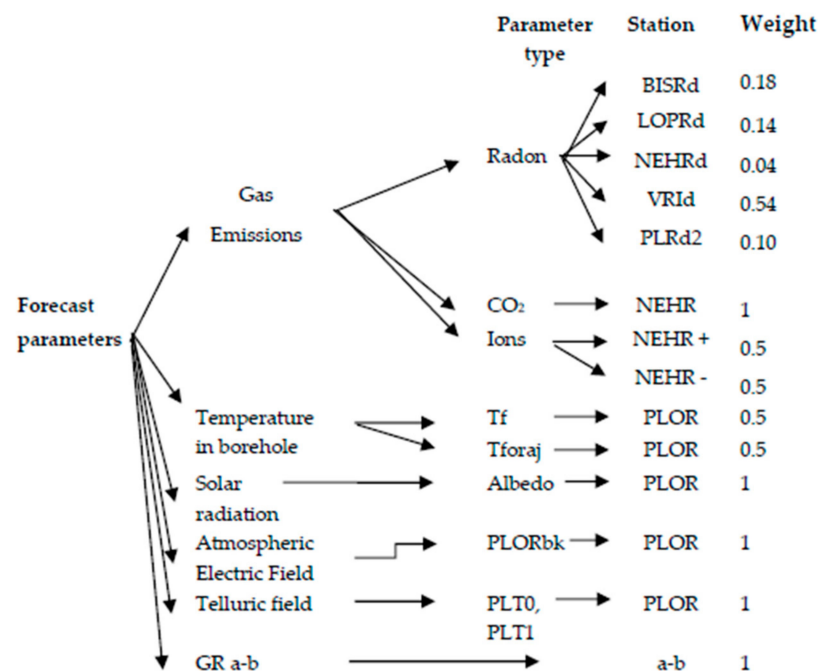


Figure 16. Logic tree of forecast parameters of Vrancea area.

The Figure 16 is a branch of a bigger logical tree that is a decision element in an OEF structure. This method allows the collaboration between the tasks of a complex application. A logical tree made for geophysical and geochemical parameters becomes a branch in a complex time-dependent seismic hazard assessment application. The collaboration can be carried out through a flexible structure, such as the one in Table 2, which can have new stations and other types of sensors. In this study we use only a part of our multidisciplinary network. A Bayesian probability assessment can be applied in this case using the data from Table 2 and adding new information to improve the time-dependent seismic hazard assessment. For example, new parameters can be added such as soil temperature, propagation of VLF-ULF-ELF (Very Low, Ultra Low, and Extremely Low frequency) radio waves, infrasound, the magnetic field and meteorological data. In addition to the measured information, the results of the analysis of other information, such as the delay time between earthquakes and the assessment of cumulative seismic energy, can also be used. A probabilistic seismic hazard assessment considering epistemic uncertainties, logical trees and a Bayesian approach is presented by Gottfried Grünthal et al. in [51].

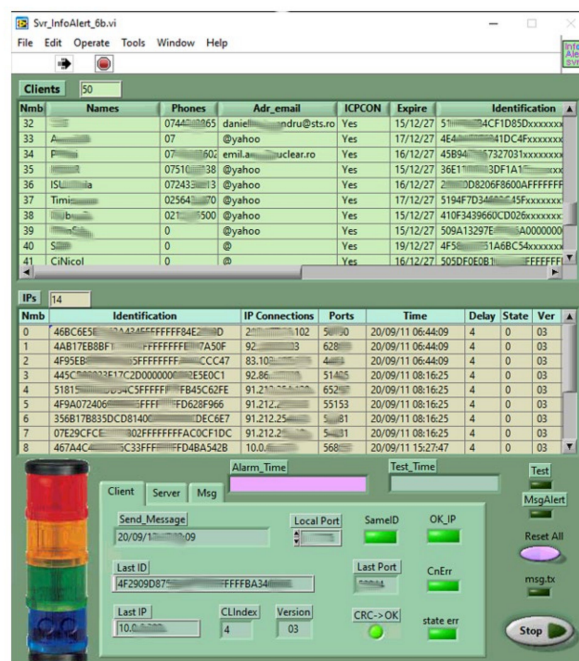
SELENA is another tool with application in seismic risk and loss assessment using a logical tree [52]. In this case the inputs are ASCII plain text files that represent tables with rows and columns. Another example to convert a logic tree into a XML file is:

```
<?xml version="1.0" encoding="UTF-8" standalone="yes"?>
<data-set xmlns:xsi="http://www.w3.org/2001/XMLSchema-instance" T1"textquotedblright">
<record>
<Type>Radon</Type>
<Station>BISRd</Station>
<Probability>0.57</Probability>
<Uncertain>4.98</Uncertain>
<Weight>0.18</Weight>
</record>
<record>
<Type>Radon</Type>
```

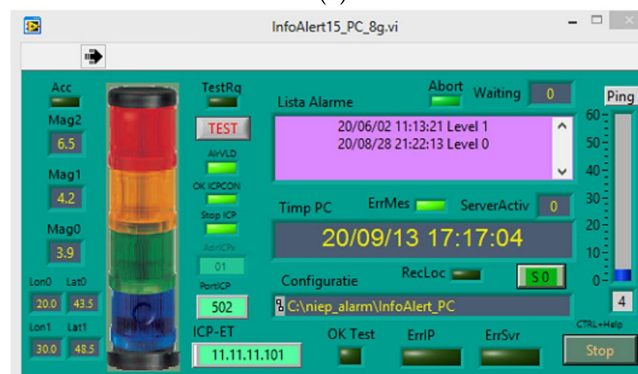
```
<Station>LOPRd</Station>
<Probability>0.29</Probability>
<Uncertain>3.93</Uncertain>
<Weight>0.14</Weight>
</record> ...
```

(5.) Decide the event state and send the information:

A probabilistic seismic hazard assessment is based on information updated by automatic detection or an offline analysis that sends the information to a logic tree. Detection must be validated by the daily and seasonal variations of the forecast parameters. A large earthquake for the Vrancea area would be 7.2R or above, but we did not have such data in our analysis. We assume that in such a case both the radon and the CO₂ levels from all stations would increase. If GR a-b would indicate variations such as the ones in Figure 12 we can declare an emergency state. The first detection level automatically sends data to a web platform. The second level, the offline analysis (Figure 12), combined with a logical tree will decide the level of emergency. This information is retrieved by a server, Figure 17a, which sends alerts to the entire network using software (b), and displays the earthquake parameters (c). The software presented in Figure 17 works in an EEW (Earthquake Early Warning) system.

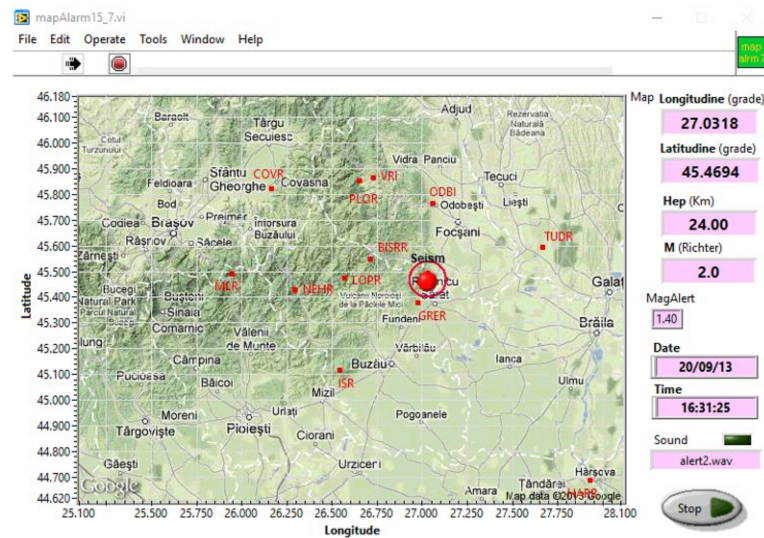


(a)



(b)

Figure 17. Cont.



(c)

Figure 17. EEW (Earthquake Early Warning) info alert network: (a) server of messages; (b) messages receiver which provides information and operates protection elements (gas blocking solenoid valve, for example); (c) displays the earthquake parameters.

The traffic light symbol from Figure 17b has 5 states: green—no warning elements; green–yellow—attention; yellow—warning; yellow–red—alert and red—major alert.

4. Discussion and Conclusions

The presented procedure highlights five steps. The first one, selecting the seismic zone, depends on the geological information we have. Gas emissions are predominant in fault zones (Figure 18). In [53], the crustal structure of the Vrancea area is shown and Figure 19 presents a resistivity tomography of a particular monitoring location, Bisoca, located on the Casin–Bisoca fault, and marked in the general plan of the faults; Figure 18. Knowing the structure of the area, an optimal positioning of the monitoring station can be achieved.

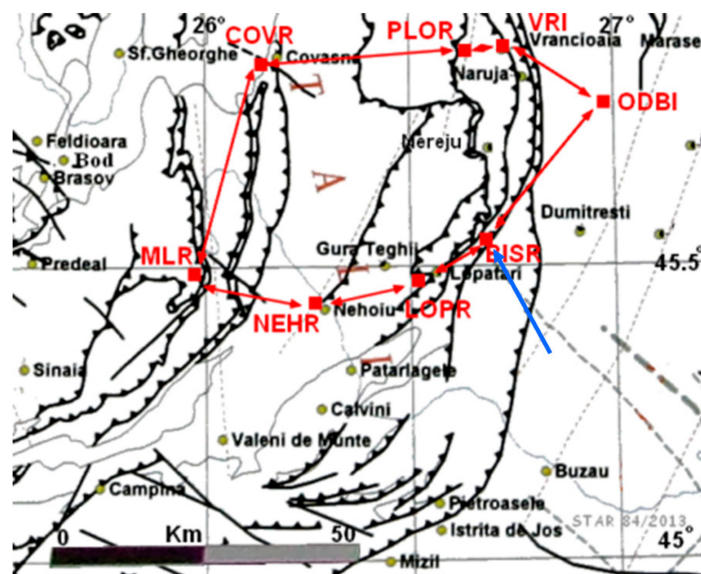


Figure 18. Monitoring network, main faults (map by C. Dinu, V. Raileanu et al.).

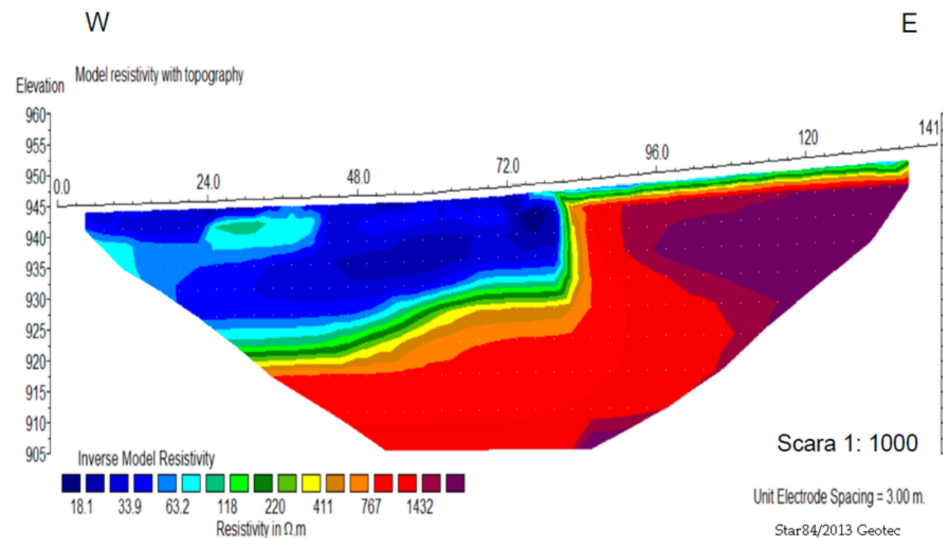


Figure 19. Model resistivity with topography in Bisoca station.

All monitoring stations have been installed in fault areas, but this is not enough. Improper installation of the sensors will affect the measurements. Figure 20 shows how the CO₂ detector was initially mounted in a room where the data was affected by staff activity (top) and in the second stage it was introduced in a box and fixed to the outside (bottom).

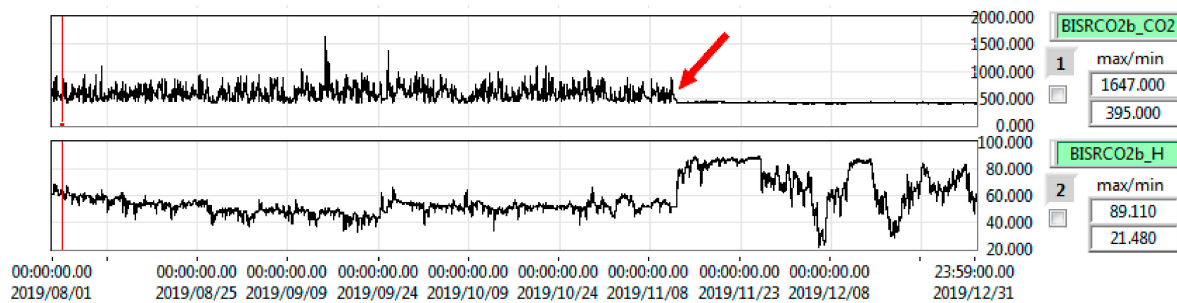


Figure 20. Dependence of measurements on the position of the CO₂ sensor in Bisoca station.

In the second phase of the procedure the daily–seasonal evolution of forecast parameters (Figures 4–11) was presented for only two years. For a correct analysis, it would have been beneficial to process larger periods of time, especially since the annual variations are affected by the global warming phenomenon. The analysis in this study focused on the correlation between gas emission and seismicity but in an OEF application many parameters are used to reduce the number of false errors. For example, N. Kastelis and K. Kourtidis in [54] analyze the correlation of an atmospheric electric field with CO₂ and S. Abbad et al. in [55] present the influence of meteorological and geological parameter variables on the concentration of radon in soil. It is more difficult to determine the interdependence between parameters such as radon activity and CO₂ flux in soil, which implies a correction of measurements [56]. Another mentioned correlation is between radon variations and the magnetic field [48]. This correlation could not be demonstrated in the case of radon measurements in the Muntele Rosu tunnel (Romania), because the humidity exhibits large oscillations dependent on water infiltrations in the mountains and on air flow from the tunnel, as presented by A. Mihai et al. [57]. For this reason the radon detector was moved to another location (code PLRd2 in Table 1). This is an example that shows how a method cannot be generalized because it depends on the specifics of the location.

We used long-term data to test the hypotheses, methods and to analyze events. In reality we have to make decisions on real-time information. In Figure 3 we have an example in which the difference between a long (e) and limited (f) period of time analysis is observed.

Regarding the next phase (3) of the procedure, Table 2 shows the result of an offline anomaly detection analysis performed by an experienced operator. If we had applied the automatic detection method based on the STA/LTA algorithm, the result would have been faster but more inaccurate. The results also depend on the number of sensors. For CO₂ or the drilling temperature Tf, only one location was used, which determines the maximum weight. The uncertain forecast time was determined using the simplest method that is the standard deviation in our case (Table 2). N. Ridler et al. in [45] combined all uncertainties using the Law of Propagation of Uncertainty (LPU) using the root-sum-squares (RSSs) method of standard deviations to give a global uncertainty (a global standard deviation).

In phase (4), the use of a logical tree can be simplified by using a voting system [33] or a decision tree that does not use weights [36]. The way in which the logical tree is made depends on the previous stages and only through experimentation can we adjust the weights of each branch.

In the final phase we must not forget that the methods are empirical in many cases and that decision-making requires responsibility if it involves departments specialized in intervention.

The main conclusion is that there is not a single precursor factor, not even a model, and that only a multidisciplinary network allows a complex analysis that reduces the number of false errors and increases the probability of a correct decision. In the case of a complex OEF system comprising a large monitoring area with different geological structures (e.g., Europe), the recommended solution is to decentralize the decision by applying the procedure described to independent zones that transmit alerts to a general information portal. In this context, the answer to the question J. Zechar wrote in his article [58], “Is Europe-wide operational earthquake forecasting (OEF) possible?”, is affirmative.

Author Contributions: Conceptualization, V.-E.T.; methodology, V.-E.T. and I.-A.M.; software, V.-E.T.; validation, I.-A.M., A.M. and C.I.; formal analysis, I.-A.M.; investigation, V.-E.T. and I.-A.M.; writing—original draft preparation, V.-E.T.; correspondent, V.N.; supervision, C.I. All authors have read and agreed to the published version of the manuscript.

Funding: This work was carried out within Nucleu Program MULTIRISC, supported by MCI, project no. 19 08 01 02/2019. This research was funded by the Romanian National Core Program Contract No.18N/2019, by the Romanian Ministry of Research and Innovation through Program. Development of the national research development system, Subprogram 1.2—Institutional Performance. Projects of Excellence Financing in RDI, Contract No.19 PFE/17.10.2018, and by the European Regional Development Fund through the Competitiveness Operational Programme 2014–2020, POC-A.1-A.1.1.1-F-2015, project Research Centre for Environment and Earth. Observation CEO-Terra, SMIS code 108109, contract No. 152/2016 and contract No. 253/2.06.2020.

Institutional Review Board Statement: Not applicable.

Informed Consent Statement: Not applicable.

Data Availability Statement: The data presented in this study are available on request from the corresponding author.

Acknowledgments: This work was carried out within Nucleu Program MULTIRISC, supported by MCI, project no. 19 08 01 02/2019 and European Union’s Horizon 2020 research and innovation programme under grant agreement No 821046. This research was funded by the Romanian Ministry of Research and Innovation through Program I—Development of the national research development system, Subprogram 1.2—Institutional Performance. Projects of Excellence Financing in RDI, Contract No.19 PFE/17.10.2018, by the Romanian National Core. Program Contract No.18N/2019; by the European Regional Development Fund through the Competitiveness Operational Programme 2014–2020, POC-A.1-A.1.1.1-F-2015, project Research Centre for Environment and Earth Observation CEO-Terra, SMIS code 108109, contract No. 152/2016 and contract No. 253/2.06.2020.

Conflicts of Interest: The authors declare no conflict of interest.

References

1. Pulinet, S. *The Possibility of Earthquake Forecasting: Learning from Nature*; Institute of Physics Publishing (Great Britain): Bristol, UK, 2018; Volume 16, ISBN 978-0-7503-1248-6.
2. Cannelli, V.; Piersanti, A.; Galli, G.; Melini, D. Italian radon monitoring network (Iron): A permanent network for near real-time monitoring of soil radon emission in Italy. *Ann. Geophys.* **2018**, *61*, 1–22. [[CrossRef](#)]
3. Piersanti, A.; Cannelli, V.; Galli, G. Long term continuous radon monitoring in a seismically active area. *Ann. Geophys.* **2015**, *58*. [[CrossRef](#)]
4. Morita, M.; Mori, T.; Yokoo, A.; Ohkura, T.; Morita, Y. Continuous monitoring of soil CO₂ flux at Aso volcano, Japan: The influence of environmental parameters on diffuse degassing. *Earth Planets Space* **2019**, *71*, 1. [[CrossRef](#)]
5. Castellana, L.; Biagi, P.F. Detection of hydrogeochemical seismic precursors by a statistical learning model. *Nat. Hazards Earth Syst. Sci.* **2008**, *8*, 1207–1216. [[CrossRef](#)]
6. Foulser-Piggott, R.; Bowman, G.; Hughes, M. A Framework for Understanding Uncertainty in Seismic Risk Assessment. *Risk Anal.* **2020**, *40*, 169–182. [[CrossRef](#)]
7. Yuçe, G.; Ugurluoğlu, D.Y.; Adar, N.; Yalcin, T.; Yaltirak, C.; Streil, T.; Oeser, V. Monitoring of earthquake precursors by multi-parameter stations in Eskisehir region (Turkey). *Appl. Geochem.* **2010**, *25*, 572–579. [[CrossRef](#)]
8. Werner, C.; Cardellini, C. Comparison of carbon dioxide emissions with fluid upflow, chemistry, and geologic structures at the Rotorua geothermal system, New Zealand. *Geothermics* **2006**, *35*, 221–238. [[CrossRef](#)]
9. Weinlich, F.H. Carbon dioxide controlled earthquake distribution pattern in the NW Bohemian swarm earthquake region, western Eger Rift, Czech Republic—gas migration in the crystalline basement. *Geofluids* **2014**, *14*, 143–159. [[CrossRef](#)]
10. Chiodini, G.; Cardellini, C.; Amato, A.; Boschi, E.; Caliro, S.; Frondini, F.; Ventura, G. Carbon dioxide Earth degassing and seismogenesis in central and southern Italy. *Geophys. Res. Lett.* **2004**, *31*, 2–5. [[CrossRef](#)]
11. Okumura, S.; Hirano, N. Carbon dioxide emission to earth's surface by deep-sea volcanism. *Geology* **2013**, *41*, 1167–1170. [[CrossRef](#)]
12. Chiodini, G.; Cardellini, C.; Lamberti, M.C.; Agosto, M.; Caselli, A.; Liccioli, C.; Tamburello, G.; Tassi, F.; Vaselli, O.; Caliro, S. Carbon dioxide diffuse emission and thermal energy release from hydrothermal systems at Copahue-Caviahue Volcanic Complex (Argentina). *J. Volcanol. Geotherm. Res.* **2015**, *304*, 294–303. [[CrossRef](#)]
13. Ármannsson, H. An overview of carbon dioxide emissions from Icelandic geothermal areas. *Procedia Earth Planet. Sci.* **2017**, *97*, 11–18. [[CrossRef](#)]
14. Ármannsson, H. Carbon Dioxide Emissions from Icelandic Geothermal Areas. *Procedia Earth Planet. Sci.* **2017**, *17*, 104–107. [[CrossRef](#)]
15. Fridriksson, T.; Kristjánsson, B.R.; Ármannsson, H.; Margrétardóttir, E.; Ólafsdóttir, S.; Chiodini, G. CO₂ emissions and heat flow through soil, fumaroles, and steam heated mud pools at the Reykjanes geothermal area, SW Iceland. *Appl. Geochem.* **2006**, *21*, 1551–1569. [[CrossRef](#)]
16. Heinicke, J.; Koch, U.; Martinelli, G. CO₂ and Radon measurements in the Vogtland area (Germany)—A contribution to earthquake prediction research. *Geophys. Res. Lett.* **1995**, *22*, 771–774. [[CrossRef](#)]
17. Jilani, Z.; Mehmood, T.; Alam, A.; Awais Muhammad and Iqbal, T. Monitoring and descriptive analysis of radon in relation to seismic activity of Northern Pakistan. *J. Environ. Radioact.* **2017**, *172*, 43–51. [[CrossRef](#)]
18. Famin, V.; Nakashima, S.; Boullier, A.M.; Fujimoto, K.; Hirono, T. Earthquakes produce carbon dioxide in crustal faults. *Earth Planet. Sci. Lett.* **2008**, *265*, 487–497. [[CrossRef](#)]
19. Sugisaki, R.; Anno, H.; Adachi, M.; Ui, H. Geochemical features of gases and rocks along active faults. *Geochem. J.* **1980**, *14*, 101–112. [[CrossRef](#)]
20. Frunzeti, N.; Baciú, C.; Etiope, G.; Pfanz, H. Geogenic emission of methane and carbon dioxide at Beciu mud volcano, (Berca-Arbănași hydrocarbon-bearing structure, Eastern Carpathians, Romania). *Carpath. J. Earth Environ. Sci.* **2012**, *7*, 159–166. [[CrossRef](#)]
21. Martinelli, G.; Albarello, D.; Mucciarelli, M. Radon Emissions from Mud Volcanos in Northern Italy—Possible Connection with Local Seismicity. *Geophys. Res. Lett.* **1995**, *22*, 1989–1992. [[CrossRef](#)]
22. Etiope, G.; Baciú, C.; Caracausi, A.; Italiano, F.; Cosma, C. Gas flux to the atmosphere from mud volcanoes in eastern Romania. *Terra Nov.* **2004**, *16*, 179–184. [[CrossRef](#)]
23. Nevinsky, V.; Nevinsky, I.; Tsvetkova, T. Measurements of soil radon in south Russia for seismological application: Methodological aspects. *Radiat. Meas.* **2012**, *47*, 281–291. [[CrossRef](#)]
24. Brustur, T.; Stănescu, I.; Macauleț, R.; Melinte-Dobrinescu, M.C. The mud volcanoes from Berca: A significant geological patrimony site of the Buzău Land Geopark (Romania). *GeoEcoMarina* **2015**, *2015*, 73–96. [[CrossRef](#)]
25. Zoran, M.; Savastru, R.; Savastru, D. Radon levels assessment in relation with seismic events in Vrancea region. *J. Radioanal. Nucl. Chem.* **2012**, *293*, 655–663. [[CrossRef](#)]
26. Woo, G.; Marzocchi, W. Operational Earthquake Forecasting and Decision-Making. In *Early Warning for Geological Disasters*; Springer: Berlin/Heidelberg, Germany, 2014; Volume 81, pp. 353–367. ISBN 978-3-642-12232-3.
27. Jordan, T.H.; Jordan, T.H.; Chen, Y.-T.T.; Gasparini, P.; Madariaga, R.; Main, I.; Marzocchi, W.; Papadopoulos, G.; Sobolev, G.; Yamaoka, K.; et al. Operational earthquake forecasting: State of knowledge and guidelines for utilization. *Ann. Geophys.* **2011**, *54*, 319–391. [[CrossRef](#)]
28. Tmkoczy, A. Understanding and parameter setting of STA/LTA trigger algorithm. *New Man. Seismol. Obs. Pract.* **2012**, *20*. [[CrossRef](#)]

29. Baillard, C.; Crawford, W.C.; Ballu, V.; Hibert, C.; Mangeney, A. An automatic kurtosis-based P-and S-phase picker designed for local seismic networks. *Bull. Seismol. Soc. Am.* **2014**, *104*, 394–409. [[CrossRef](#)]
30. Agletdinov, E.; Merson, D.; Vinogradov, A. A new method of low amplitude signal detection and its application in acoustic emission. *Appl. Sci.* **2020**, *10*, 73. [[CrossRef](#)]
31. Vassallo, M.; Satriano, C.; Lomax, A. Automatic picker developments and optimization: A strategy for improving the performances of automatic phase pickers. *Seismol. Res. Lett.* **2012**, *83*, 541–554. [[CrossRef](#)]
32. Banfill Software Engineering. Available online: https://banfill.net/?page_id=16, Banfill (accessed on 15 September 2020).
33. Trnkoczy, A. Understanding and Setting STA/LTA Trigger Algorithm Parameters for the K2. *Appl Note* **1998**, *41*, 16–20.
34. Allen, R. Automatic phase pickers: Their present use and future prospects. *Bull. Seismol. Soc. Am.* **1982**, *72*, S225–S242.
35. Chi-Durán, R.; Comte, D.; Díaz, M.; Silva, J.F. Automatic detection of P- and S-wave arrival times: New strategies based on the modified fractal method and basic matching pursuit. *J. Seismol.* **2017**, *21*, 1171–1184. [[CrossRef](#)]
36. Gregori, A.; Zmazek, B.; Deroski, S.; Torkar, D.; Vaupoti, J. Radon as an Earthquake Precursor—Methods for Detecting Anomalies. In *Earthquake Research and Analysis—Statistical Studies, Observations and Planning*; IntechOpen: London, UK, 2012; pp. 179–196, ISBN 978-953-51-0134-5. [[CrossRef](#)]
37. Kijko, A. Estimation of Gutenberg-Richter b-value without Level of Completeness Apparent (Observed) Frequency-Magnitude Distribution Proposed Parametrization. *Annu. Meet. SSA* **2016**, 19–20. [[CrossRef](#)]
38. Utsu, T. A method for determining the value of b in a formula $\log N = a - bM$ showing the magnitude-frequency relation for earthquakes. *Geophys. Bull. Hokkaido Univ.* **1965**, *13*, 99–103. [[CrossRef](#)]
39. Enescu, B.; Enescu, D.; Ito, K. Values of b and p: Their variations and relation to physical processes for earthquakes in Japan and Romania. *Rom. Rep. Phys.* **2011**, *56*, 590–608.
40. Bilim, F. The correlation of b-value in the earthquake frequency-magnitude distribution, heat flow and gravity data in the Sivas Basin, central eastern Turkey. *Bitlis Eren Univ. J. Sci. Technol.* **2019**, *9*, 11–15. [[CrossRef](#)]
41. Gutenberg, B.; Richter, C.F. Earthquake magnitude, intensity, energy, and acceleration: (Second paper). *Bull. Seismol. Soc. Am.* **1956**, *46*, 105–145.
42. Dobrovolsky, I.P.; Zubkov, S.I.; Miachkin, V.I. Estimation of the size of earthquake preparation zones. *Pure Appl. Geophys. Pageoph* **1979**, *117*, 1025–1044. [[CrossRef](#)]
43. Tchorz-Trzeciakiewicz, D.E.; Solecki, A.T. Seasonal variation of radon concentrations in atmospheric air in the Nowa Ruda area (Sudety Mountains) of southwest Poland. *Geochem. J.* **2011**, *45*, 455–461. [[CrossRef](#)]
44. Süer, S.; Wiersberg, T.; Güleç, N.; Erzinger, J.; Parlaktuna, M. Geochemical Monitoring of the Seismic Activities and Noble Gas Characterization of the Geothermal Fields along the Eastern Segment of the Büyük Menderes Graben SETTING AND RECENT. In *Proceedings of the World Geothermal Congress, Bali, Indonesia, 25–30 April 2010*; pp. 25–29.
45. Ridler, N.; Lee, B.; Martens, J.; Wong, K. Measurement uncertainty, traceability, and the GUM. *IEEE Microw. Mag.* **2007**, *8*, 44–53. [[CrossRef](#)]
46. Kitov, I.O.; Sanina, I.A.; Sergeev, S.S.; Nesterkina, M.A.; Konstantinovskaya, N.L. Detection, Estimation of Magnitude, and Relative Location of Weak Aftershocks Using Waveform Cross-Correlation: The Earthquake of August 7, 2016, in the Town of Mariupol. *Seism. Instrum.* **2018**, *54*, 158–174. [[CrossRef](#)]
47. Rusov, V.D.; Maksymchuk, V.Y.; Ilić, R.; Pavlovyh, V.M.; Bakhmutov, V.G.; Saranuk, D.N.; Vaschenko, V.M.; Skvarč, J.; Hanžič, L.; Rusov, V.D.; et al. The Peculiarities of Cross-Correlation between Two Secondary Precursors—Radon and Magnetic Field Variations, Induced by Tectonic Activity V.D. *Ukr. Antarct. J.* **2006**, 160–181. [[CrossRef](#)]
48. Vaughan, N.; Lenton, T. Interactions between reducing CO₂ emissions, CO₂ removal and solar radiation management. *Philos. Trans. R. Soc. A Math. Phys. Eng. Sci.* **2012**, *370*, 4343–4364. [[CrossRef](#)] [[PubMed](#)]
49. Toader, V.E.E.; Biagi, P.F.; Moldovan, I. Evaluation of the Solar Radiation in a Seismic Zone. *IOP Conf. Ser. Earth Environ. Sci.* **2019**, *362*, 012069. [[CrossRef](#)]
50. Bommer, J.J. On the Use of Logic Trees for Ground-Motion Prediction Equations in Seismic-Hazard Analysis. *Bull. Seismol. Soc. Am.* **2005**, *95*, 377–389. [[CrossRef](#)]
51. Grünthal, G.; Stromeyer, D.; Bosse, C.; Cotton, F.; Bindi, D. The probabilistic seismic hazard assessment of Germany—Version 2016, considering the range of epistemic uncertainties and aleatory variability. *Bull. Earthq. Eng.* **2018**, *16*, 4339–4395. [[CrossRef](#)]
52. Molina, S.; Lang, D.H.; Lindholm, C.D. SELENA—An open-source tool for seismic risk and loss assessment using a logic tree computation procedure. *Comput. Geosci.* **2010**, *36*, 257–269. [[CrossRef](#)]
53. Hauser, F.; Raileanu, V.; Fielitz, W.; Bala, A.; Prodehl, C.; Polonic, G.; Schulze, A. VRANCEA99-The crustal structure beneath the Southeastern Carpathians and the Moesian platform from a seismic refraction profile in Romania. *Tectonophysics* **2001**, *340*, 233–256. [[CrossRef](#)]
54. Kastelis, N.; Kourtidis, K. Characteristics of the atmospheric electric field and correlation with CO₂ at a rural site in southern Balkans. *Earth Planets Space* **2016**, *68*, 1–15. [[CrossRef](#)]
55. Abbad, S.; Robe, M.C.; Bernat, M.; Labed, V. Influence of meteorological and geological parameter variables on the concentration of radon in soil gases: Application to seismic forecasting in the Provence-Alpes-Cote d’Azur region. *Environ. Geochem. Health* **1995**, *16*, 35–48.
56. Lane-Smith, D.; Sims, K.W.W. The effect of CO₂ on the measurement of ²²⁰Rn and ²²²Rn with instruments utilising electrostatic precipitation. *Acta Geophys.* **2013**, *61*, 822–830. [[CrossRef](#)]

-
57. Mihai, A.; Moldovan, I.A.; Toader, V.E.; Petrescu, L.; Partheniu, R. Geomagnetic Field Behaviour at Muntele Rosu (Romania) and Anomaly Interpretation. *IOP Conf. Ser. Earth Environ. Sci.* **2019**, *221*, 1–10. [[CrossRef](#)]
 58. Zechar, J.D.; Marzocchi, W.; Wiemer, S. Operational earthquake forecasting in Europe: Progress, despite challenges. *Bull. Earthq. Eng.* **2016**, *14*, 2459–2469. [[CrossRef](#)]